Soft Matter

Cite this: *Soft Matter*, 2012, **8**, 7904

www.rsc.org/softmatter

PAPER

Effect of interfacial air entrapment on the adhesion of bio-inspired mushroom-shaped micro-pillars

Giuseppe Carbone*[a] and Elena Pierro[b]

Received 27th March 2012, Accepted 18th May 2012
DOI: 10.1039/c2sm25715g

Recent theoretical and experimental studies have shown that mushroom shaped micro-pillars exhibit strongly enhanced adhesive performance in comparison to other pillar shapes. However, in the presence of interfacial impurities (*e.g.* solid particles or air bubbles) the adhesive strength could drastically drop. In this paper we theoretically investigate the effect of the entrapment of micro-bubbles of air at the interface between the mushroom shaped micro-pillar and a rigid substrate on the adhesive performance. We calculate the critical pull-off stress as a function of the initial volume of the entrapped air, and compare these results with those obtained when, instead of air, small external solid particles are entrapped at the interface. Our results show that the presence of entrapped air is more critical since it strongly reduces the suction effect. The critical stress, indeed, is about 35–40% smaller than the value observed in the case of solid particles, thus resulting in a considerable reduction of the adhesive performance of the mushroom shaped pillar.

1 Introduction

Microstructured adhesive surfaces, inspired by some biological attachment systems present in Nature (*e.g.* Gecko foot pad), often exhibit extremely high adhesive performance.[1–11] The secret of this amazing behavior is mainly related to their fibrillar hierarchical geometry that makes these structures very compliant [*i.e.* they store a negligible amount of repulsive elastic energy; however they are usually constituted mainly of a relatively stiff material, the β-keratin (elastic modulus $E \approx 1$ GPa)] and splits the contact with the underlying surface in a very large number of very small spots.[12–23] However, examples exist in Nature, *e.g.* the attachment pad of the males of some beetle species from the family Chrysomelidae, which do not present a hierarchical geometry as in the case of Geckos, but are surfaces covered with mushroom-shaped microstructures.[24–26] In such cases the shape of the terminal plate is crucial for the achievement of high adhesive strength values of the bio-inspired artificial surface.[27–30] In particular, experimental observations[26,31,32] have shown that mushroom shaped microstructures [Fig. 1(a)] strongly outperform, in terms of adhesive properties, surfaces covered with miniaturized flat-punches [Fig. 1(b)] made of the same material (polyvinylsiloxane (PVS), Young's modulus $E = 3$ MPa). Recently the authors[27,28] have clarified the physical mechanism which provides mushroom shaped micro-pillars with superior adhesive performance if compared to simple flat punch shaped micro-pillars. Optimal mushroom shapes, in particular, usually detach because of the propagation of existing interfacial defects, *e.g.* dust particles or solid impurities (mode II debonding).[27,28,32] Flat punch shaped micropillars or non-optimized mushroom shaped micropillars may present, on the contrary, much lower adhesive performance since they usually debond because of crack propagation from the external perimeter towards the inner region of the pillar (mode I mechanism).[27,28] However, even on perfectly clean surfaces, where the adhesive strength of the pillar is expected to be very large, micro–nano-bubbles of air might form during the initial approach of the micropillar to the substrate. These bubbles may remain entrapped at the interface[33,34] and strongly reduce the adhesive performance of the system. In this paper, we focus on this aspect of micro-pillar adhesion. With this scope in mind, we first calculate the interfacial energy of the system, and then we determine the equilibrium conditions depending on the applied tractive stress and initial size of the entrapped air bubble. We show that the system may exhibit stable or unstable equilibrium states separated by an energy barrier ΔU_B. By increasing the external applied tractive stress the energy barrier ΔU_B constantly decreases and vanishes at the critical stress (the so-called pull-off stress) σ_{cr}, which destabilizes the air bubble and causes the detachment of the pillar. Comparing this critical debonding stress σ_{cr} to the one caused by the presence of solid defects (of same size) at the interface we find a reduction of about 35–40%, which therefore must be taken into account when assessing the performance of these microstructured adhesives.

[a]*TriboLAB - Dipartimento di Ingegneria Meccanica e Gestionale - Politecnico di Bari, V.le Japigia 182, 70126 Bari, Italy; Web: http://tribolab.poliba.it. E-mail: carbone@poliba.it; Fax: +39 080 596 2746; Tel: +39 080 596 2746*
[b]*Università degli Studi della Basilicata, Dipartimento di Ingegneria e Fisica dell'Ambiente, 85100 Potenza, Italy*

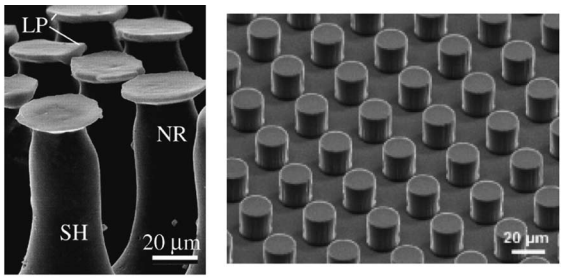

Fig. 1 A SEM image of microfabricated PVS mushroom shaped pillars (courtesy of prof. Gorb): LP, contact plate lip; NR, narrow neck; SH, pillar shaft, (a); a SEM image of a microstructured surface with flat punch (adapted from ref. 8), (b).

2 The total interfacial energy of the system

In order to carry out the analysis we need to precisely calculate the total energy change of the system when a bubble of air is present at the interface. We assume that the bubble of air is much smaller than the diameter and height of the pillar so that one can treat the pillar as an elastic half-space in contact with a rigid flat surface. Assuming isothermal conditions and a constant uniform asymptotic tractive stress σ, the equilibrium of the system can be sought by requiring that the total free energy at the interface (*i.e.* the total interfacial Gibbs energy) is stationary. Given the defect size and assuming the material linear elastic, the calculation of the energy change of the system must consider four different contributions (see also Appendix A for a different derivation): (i) the contribution to the interfacial elastic energy due to the asymptotic applied uniform tractive stress σ, (ii) the contribution to the interfacial elastic energy due the air pressure p, (iii) the internal energy of the air bubble, and (iv) the variation of surface energies due to the presence of van der Waals forces. Let us focus on the first two contributions (see Fig. 2). In the former case [Fig. 2(a) and (b)] the variation of elastic energy which occurs as the interfacial stress on the circular patch of fixed radius a is released from the uniform asymptotic value σ to zero is

$$(\Delta U_{el})_1 = U_1 - U_0 = -\frac{1}{2}\sigma V_1 \tag{1}$$

In the second case [Fig. 2(c) and (d)], the increase of air bubble pressure from zero to p causes a further increase of the volume of the bubble from the value V_1 to the value V. As a consequence the interfacial elastic energy this time increases the quantity

$$(\Delta U_{el})_2 = \frac{1}{2}p(V - V_1) \tag{2}$$

The total variation of the elastic energy is then

$$\Delta U_{el} = -\frac{1}{2}\sigma V_1 + \frac{1}{2}p(V - V_1) \tag{3}$$

Now observe that, because of linear elasticity, the volume of the void is proportional to the uniform applied stress, *i.e.* $V_1 = k\sigma$, $V = k(\sigma + p)$, and $V - V_1 = kp$,[35] where $k = 8a^3/(3E^*)$ and $E^* = E/(1 - \nu^2)$, E being Young's modulus and ν Poisson's ratio. As a consequence one obtains

$$\Delta U_{el} = \frac{1}{2}(p - \sigma)V = -\frac{4a^3}{3E^*}(\sigma^2 - p^2) \tag{4}$$

Besides the elastic energy one should also consider the contribution to the total energy due to the change of adhesion energy $\Delta U_{ad} = \pi a^2 \Delta\gamma$ ($\Delta\gamma$ being Duprè energy of adhesion and a the radius of the detached area[35]) and the contribution of the free energy U_A of the entrapped air under isothermal conditions. Assuming the ideal gas law, *i.e.* $pV = nRT$ (where n is the number of moles, R the ideal gas constant and T the absolute temperature), and isothermal conditions, we write $U_A = -nRT\ln(V/V_0) = -p_0V_0\ln(V/V_0)$, with p_0 and V_0 the initial pressure and volume of the bubble which has been entrapped during the approach of the pillar to the rigid flat and clean substrate. To characterize the initial size of the bubble (*i.e.* the number of moles of entrapped air) we may define an initial equivalent hemispherical void size with radius a_0 satisfying the relation $V_0 = (2/3)\pi a_0^3$. Summing up the different energy contributions the total energy change becomes

$$\Delta U_{tot} = -\frac{4a^3}{3E^*}(\sigma^2 - p^2) + \pi a^2\Delta\gamma - p_0V_0\ln(V/V_0) \tag{5}$$

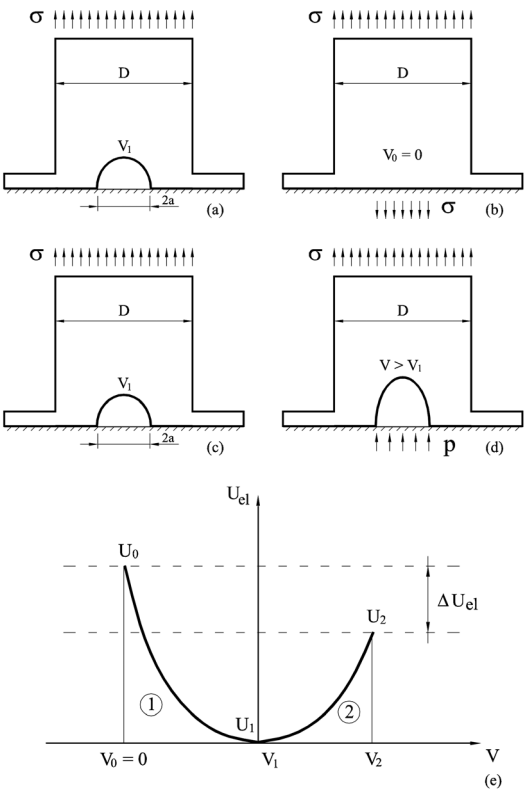

Fig. 2 The void formation at the interface of a mushroom shaped pillar of diameter D (cross-sectional area $A = \pi D^2/4$) and a rigid flat substrate. The pillar is subjected to an external tensile stress σ. The non-contact area is circular with radius a. The void formation process involves different steps: the variation of elastic energy from (a) to (b) is $\sigma V_1/2$, whereas the variation of elastic energy from (c) to (d), due to the action of bubble pressure p, is $(V - V_1)p/2$. A schematic view of the elastic energy change is represented in (e). Because of linear elasticity one also has $V_1 = k\sigma$, $V = k(\sigma + p)$, and $V - V_1 = kp$, with $k = 8a^3/(3E^*)$.

Besides eqn (5) we need two additional equations:

$$pV = p_0 V_0 \tag{6}$$

and

$$V = \frac{8a^3}{3E^*}(\sigma + p) \tag{7}$$

Eqn (6) and (7) allow us to calculate the quantity V and p as a function of the radius a of the non-contact circular area. Therefore, the total energy change ΔU_{tot} given by eqn (5) finally depends only on the applied constant stress σ and the size of the voids a. By following a similar approach as in JKR theory,[38] requiring that $\partial \Delta U_{tot}/\partial a|_\sigma = 0$ allows one to calculate the values of a at equilibrium, given the applied uniform stress σ. The critical pull-off stress σ_{cr}, which destabilizes the defect and causes the detachment of the pillar from the rigid flat substrate, is determined by requiring that at equilibrium the relation $\partial^2 \Delta U_{tot}/\partial a^2|_\sigma = 0$ is also satisfied.

The above equations can be rephrased in a dimensionless form. To this end let us define the adhesion length $\delta = \Delta\gamma/E^*$ and the dimensionless quantities $\tilde{\sigma} = \sigma/E^*$, $\tilde{p} = p/E^*$, $\tilde{a} = a/\delta$, and $\tilde{V} = V/\delta^3$. The dimensionless total energy change of the system is therefore

$$\Delta\tilde{U}_{tot} = \left(\frac{\Delta U_{tot}}{\delta^3 E^*}\right) = -\frac{4}{3}\tilde{a}^3(\tilde{\sigma}^2 - \tilde{p}^2) + \pi\tilde{a}^2 - \tilde{p}_0\tilde{V}_0 \ln\left(\frac{\tilde{V}}{\tilde{V}_0}\right) \tag{8}$$

where

$$\tilde{V} = \frac{8}{3}(\tilde{\sigma} + \tilde{p})\tilde{a}^3 \tag{9}$$

and

$$\tilde{p}\tilde{V} = \tilde{p}_0\tilde{V}_0 \tag{10}$$

Solving eqn (9) and (10) gives

$$\tilde{p} = \frac{1}{2}\left(-\tilde{\sigma} + \sqrt{\tilde{\sigma}^2 + \pi\tilde{p}_0\left(\frac{\tilde{a}_0}{\tilde{a}}\right)^3}\right) \tag{11}$$

$$\tilde{V} = \frac{4}{3}\tilde{a}^3\left(\tilde{\sigma} + \sqrt{\tilde{\sigma}^2 + \pi\tilde{p}_0\left(\frac{\tilde{a}_0}{\tilde{a}}\right)^3}\right) \tag{12}$$

3 The critical stress and the critical air bubble size

We assume that the environment pressure is 1 bar, so that the initial pressure of the entrapped air bubble is 0.1 MPa. We also notice that the asymptotic applied stress $\sigma = \sigma_0 - p_0$, where $\sigma_0 = F/A$ is the external applied average stress, F the applied load and A the cross-sectional area of the pillar. Fig. 3 shows the total dimensionless energy change $\Delta\tilde{U}_{tot}$ as a function of the dimensionless radius $\tilde{a}$, for different values of the initial dimensionless size $\tilde{a}_0$ of the void. In our calculations we have used $\sigma = 0.2$ MPa (*i.e.* $\sigma = 0.3$ MPa), $\Delta\gamma \approx 16$ mJ m^{-2}, $E = 3$ MPa and $\nu = 0.5$. The figure shows that for any value of $\tilde{a}_0$, two equilibrium conditions exist, *i.e.* the stable state (energy minimum) and the unstable state (energy maximum). However, as expected, when the asymptotic

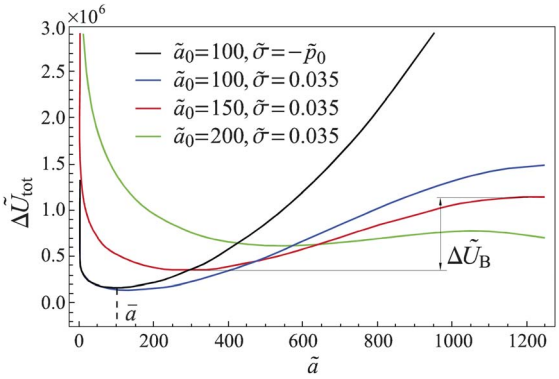

Fig. 3 The dimensionless total energy $\Delta\tilde{U}_{tot}$ as a function of the radius of the detached area $\tilde{a}$, for three different values of the initial radius $\tilde{a}_0$, given the same value of dimensionless stress $\tilde{\sigma} = 0.035$ (blue, red and green curves). Increasing $\tilde{a}_0$ determines a decrease of the energy barrier $\Delta\tilde{U}_B$ between the stable and unstable equilibrium states. The solid black curve represents the total energy as a function of $\tilde{a}$ when the pillar is subjected to the environment pressure only, *i.e.* $\tilde{\sigma} = -\tilde{p}_0$, and for $\tilde{a}_0 = 100$. Note that in this case there is only one equilibrium condition at $\tilde{a} = \bar{a}$ which is necessarily stable.

applied stress is zero or even negative only a stable equilibrium state must be present (see the black line in Fig. 3 with $\tilde{a}_0 = 100$ and $\tilde{\sigma} = -\tilde{p}_0$, *i.e.* $\tilde{\sigma}_0 = 0$). When an external stress $\sigma > 0$ is applied, an energy barrier must be exceeded in order to destabilize the system. The energy barrier $\Delta\tilde{U}_B$ is defined as the difference between the energy value of the unstable equilibrium state and the energy value of the stable equilibrium state. From Fig. 3, given the same applied stress, one observes that the energy barrier $\Delta\tilde{U}_B$ decreases as the initial radius $\tilde{a}_0$ of the bubble (*i.e.* its initial volume) is increased. When $\Delta\tilde{U}_B = 0$, *i.e.* when $\partial \Delta U_{tot}/\partial a|_\sigma = 0$ and $\partial^2 \Delta U_{tot}/\partial a^2|_\sigma = 0$, the critical defect size $(\tilde{a}_0)_{cr}$ is found which prevents the pillar from adhering to the substrate.

Given the initial defect size $\tilde{a}_0$, one may also analyze what happens when the applied stress σ is increased. In particular, Fig. 4 shows that, for a fixed value of the radius $\tilde{a}_0$ (we have considered $a_0 = 0.6$ μm, *i.e.* $\tilde{a}_0 = 150$), when the applied stress σ increases an unstable equilibrium state appears, which is again separated from the corresponding stable equilibrium by an

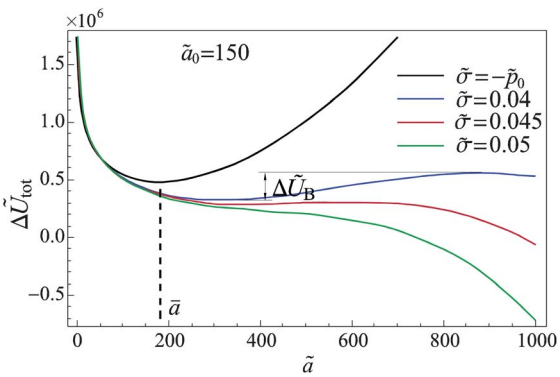

Fig. 4 The dimensionless total energy $\Delta\tilde{U}_{tot}$ as a function of the radius of the detached area $\tilde{a}$, for four different values of the applied stress $\tilde{\sigma}$, and for $\tilde{a}_0 = 150$. Increasing $\tilde{\sigma}$ determines a decrease of the energy barrier $\Delta\tilde{U}_B$ between the stable and unstable equilibrium states until it vanishes and the air bubble is destabilized.

energy barrier $\Delta\tilde{U}_B$. As the stress $\tilde{\sigma}$ is further increased, the energy barrier $\Delta\tilde{U}_B$ decreases and vanishes at a certain stress level $\tilde{\sigma}_{cr}$ (the so-called critical pull-off stress) at which the air bubble of initial size $\tilde{a}_0$ is destabilized and the pillar detaches from the substrate.

In Fig. 5 both the stable and the unstable equilibrium values $\tilde{a}_{eq}$ of the air bubble size are shown as functions of the applied stress $\tilde{\sigma}$, for different values of $\tilde{a}_0$. The upper branches represent the unstable states; the lower branches are the stable states. By increasing the stress $\tilde{\sigma}$, the two values of $\tilde{a}_{eq}$ tend to approach each other, until they coincide at $\tilde{\sigma} = \tilde{\sigma}_{cr}$. The dash-dotted line in Fig. 5 gives the critical stress $\tilde{\sigma}_{cr}$ for different values of the initial radius $\tilde{a}_0$ of the bubble, of course larger entrapped bubbles, *i.e.* larger values of $\tilde{a}_0$ lead to a reduction of the critical pull-off force $\tilde{\sigma}_{cr}$.

4 Solid defects *vs.* air bubbles

In many cases solid defects (dust particles, impurities, *etc.*) may be present at the interface between the adhering pillar and the substrate. In such cases, the authors have shown recently[27,28] that mushroom shaped pillars usually detach because of the propagation of these interfacial defects (mode II debonding mechanism) when the stress level becomes $\sigma_{II} = [\pi\Delta\gamma E^*/(2a_S)]^{1/2}$, where a_S is the solid defect size. It is, hence, interesting to compare this critical value σ_{II} with the critical pull-off stress σ_{cr} obtained in the case of a bubble of air entrapped at the interface. The comparison must be carried out assuming that, at $\tilde{\sigma} = -\tilde{p}_0$ (*i.e.* $\tilde{\sigma}_0 = 0$), the (dimensionless) size $\bar{a}$ of the air bubble at equilibrium is identical to the (dimensionless) solid defect size, *i.e.* $\bar{a} = \tilde{a}_S$. Fig. 6 compares the critical stress $\tilde{\sigma}_{0cr} = \tilde{\sigma}_{cr} + \tilde{p}_0$ in the two cases as a function of the radius $\bar{a}$. We observe that in the case of air bubble the debonding stress $\tilde{\sigma}_{0cr}$ is always significantly smaller than the one obtained in the case of solid defects with a reduction of about 35–40% over the entire range of defect size considered in the calculation, *i.e.* $\bar{a} = \tilde{a}_S = 0.4$–$4$ μm. Indeed, micro-air bubbles weaken the adhesive link between the pillar and the rigid substrate more than the presence of external particles, since their gas pressure exerts an additional debonding force and reduces the suction effect which contributes to keep the pillar in contact with the substrate. This represents a practical problem during fast attaching–detaching of these kinds of microstructures, since in this case the entrapment of air can hardly be avoided.

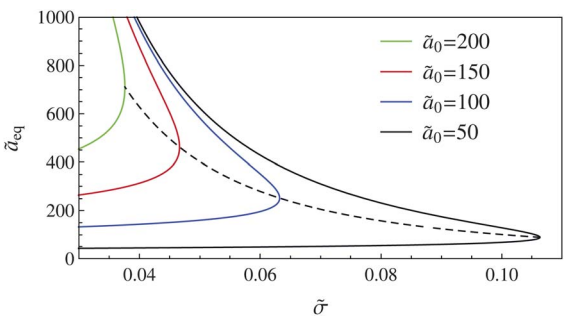

Fig. 5 The dimensionless stable and unstable equilibrium values $\tilde{a}_{eq}$ as functions of the external applied stress $\tilde{\sigma}$, for different initial radii $\tilde{a}_0$ of the air bubble. As the load is increased, the upper (unstable) $\tilde{a}_{eq}$ values and the lower (stable) $\tilde{a}_{eq}$ values approach each other until they coincide in correspondence of the critical stress $\tilde{\sigma}_{cr}$ (dash-dotted line).

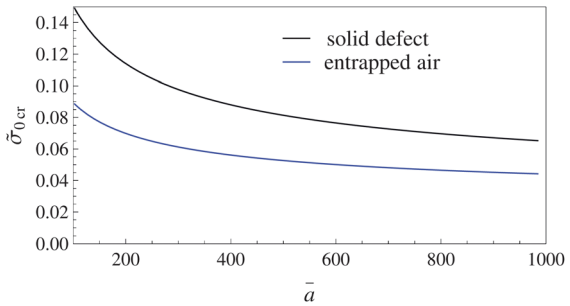

Fig. 6 The dimensionless external critical stress $\tilde{\sigma}_{0cr} = \tilde{\sigma}_0 + \tilde{p}_0$ as a function of the air bubble or solid particle size $\bar{a}$ (see text for more details). The blue curve refers to the air bubble case, the black curve to the interfacial solid particle case.

5 Conclusions

In this paper, we investigate the influence of interfacial micro-bubbles of air on the adhesive properties of micro-mushroom-shaped pillars. We show that, in the absence of an applied load, the micro-bubble remains in stable equilibrium. However as soon as an external tractive stress is applied to the pillar, an unstable equilibrium condition appears. This means that a critical pull-off stress exists which destabilizes the air bubble and causes the complete detachment of the pillar from the substrate. We have calculated this critical pull-off stress and showed how it depends on the initial volume of entrapped air. Of course, increasing the amount of entrapped air leads to a significant reduction of the pull-off stress. Interestingly our results have highlighted that the air bubbles at the interface are more critical than the presence of interfacial solid defects of the same size. It follows that to achieve the highest adhesive performance the approach of the pillar to the substrate must be carried out very carefully, to avoid entrapment of air at the interface.

A The free energy at the interface

Here we present a different and thermodynamically rigorous derivation of eqn (5). To this purpose let us consider the system shown in Fig. 7 where the bottom (initially flat) surface of an elastic half-space is glued to a rigid plate except for a circular region of radius a. Let us displace the rigid plate of a quantity u_0 (see Fig. 7) so that a small void is formed at the interface. Assume that the air pressure in the void is p. Our scope is to calculate the elastic energy of the system. To this end let us first observe that one of the authors has shown[36] that the contact problem may have an equivalent formulation in terms of interfacial elastic energy, *i.e.* in terms of the amount of elastic energy stored at the interface as a consequence of local interfacial deformations. Accordingly, the elastic interfacial energy is[36]

$$\mathscr{E} = \frac{1}{2}\int d^2x\sigma_{zz}(\boldsymbol{x})\left[u_z(\boldsymbol{x}) - \langle u_z(\boldsymbol{x})\rangle\right] \tag{13}$$

where $\boldsymbol{x}$ is the in-plane position vector, $\sigma_{zz}(\boldsymbol{x})$ is the non-uniform normal interfacial stress, $u_z(\boldsymbol{x})$ is the local normal displacement of the surface, and $\langle u(\boldsymbol{x})\rangle$ is the average displacement at the interface (the symbol $\langle\ \rangle$ is the average operator). Considering that

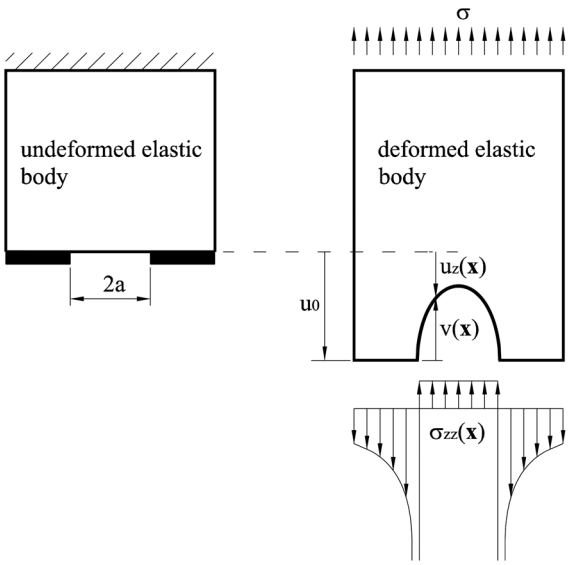

Fig. 7 The displacement, gap and stress distributions involved in the calculation of the free interfacial energy.

because of force balance the uniform stress σ at infinity is $\sigma = \langle \sigma_{zz}(\boldsymbol{x}) \rangle$ one can rephrase eqn (13) as

$$\mathscr{E} = \frac{1}{2} \int d^2x \left[\sigma_{zz}(\mathbf{x}) - \sigma \right] u_z(\mathbf{x}) \tag{14}$$

Now let us define (see Fig. 7) the gap distribution $v(\boldsymbol{x})$ as $v(\boldsymbol{x}) = u_0 - u_z(\boldsymbol{x})$. Of course $v(\boldsymbol{x}) \neq 0$ on the circular region of radius a, whereas it vanishes elsewhere. Using $v(\boldsymbol{x})$ and considering that $\sigma_{zz}(\boldsymbol{x}) = -p$ for $|\boldsymbol{x}| < a$, eqn (14) becomes

$$\mathscr{E} = \frac{1}{2}(p + \sigma)V \tag{15}$$

where $V = \int d^2x v(\boldsymbol{x})$ is the volume of the air bubble. The total Helmholtz free interfacial energy $\mathscr{F}$ is then the sum of the elastic interfacial energy, the free internal energy $U_A = -p_0 V_0 \ln(V/V_0)$ of the entrapped air, and the surface energy, *i.e.*

$$\mathscr{F}(V,a) = \mathscr{E}(V,a) + U_A(V) + \pi a^2 \Delta\gamma \tag{16}$$

From thermodynamics one concludes that under constant bubble volume V the equilibrium of the system corresponds to the stationary values of the energy $\mathscr{F}$. However, in our analysis we, instead, keep the asymptotic load constant $\langle \sigma(\boldsymbol{x}) \rangle = \sigma$. In this case the equilibrium states of the system correspond to the stationary values of the interfacial Gibbs energy $\mathscr{G}(\sigma,a)$. Following the standard approach of thermodynamics,[37] we obtain $\mathscr{G}(\sigma,a)$ by enforcing a Legendre transformation, *i.e.*

$$\mathscr{G}(\sigma,a) = \mathscr{F}(V,a) - \left. \frac{\partial \mathscr{F}}{\partial V} \right|_a V \tag{17}$$

Observing that $\partial \mathscr{E}/\partial V|_a = p + \sigma$ and $\partial U_A/\partial V|_a = -p$, one yields the required expression for the interfacial Gibbs energy $\mathscr{G}$, *i.e.*

$$\mathscr{G}(\sigma,a) = \frac{1}{2}(p - \sigma)V + U_A + \pi a^2 \Delta\gamma \tag{18}$$

which is the same as the one obtained in eqn (5).

The authors thank the financial support of Regione Apulia (Italy) within the agreement "Accordo di Programma Quadro in Materia di Ricerca Scientifica - II Atto Integrativo" project TRASFORMA code n. 28 signed on Dec. 3, 2009.

References

1 C. Majidi, R. E. Groff, Y. Maeno, B. Schubert, S. Baek, B. Bush, R. Maboudian, N. Gravish, M. Wilkinson, K. Autumn and R. S. Fearing, *Phys. Rev. Lett.*, 2006, **97**, 076103.
2 A. K. Geim, *et al.*, *Nat. Mater.*, 2003, **2**(7), 461.
3 T. Kim, H. E. Jeong, K. Y. Suh and H. H. Lee, *Adv. Mater.*, 2009, **21**, 2276–2281.
4 H. Lee, B. P. Lee and P. B. Messersmith, *Nature*, 2007, **448**, 338–342.
5 R. Spolenak, S. Gorb and E. Artz, *Acta Biomater.*, 2005, **1**, 5–13.
6 A. del Campo, C. Greiner and E. Arzt, *Langmuir*, 2007, **23**, 10235–10243.
7 C. Greiner, R. Spolenak and E. Arzt, *Acta Biomater.*, 2009, **5**, 597–606.
8 C. Greiner, A. del Campo and E. Arzt, *Langmuir*, 2007, **23**, 3495–3502.
9 B. N. J. Persson, *Wear*, 2003, **254**, 832–834.
10 B. N. Persson and S. Gorb, *J. Chem. Phys.*, 2003, **119**, 11437–11444.
11 K. Autumn, Y. A. Liang, S. T. Hsleh, W. Zesch, W. P. Chan, T. W. Kenny, R. Fearilng and R. J. Full, *Nature*, 2000, **405**, 681–686.
12 G. Carbone, L. Mangialardi and B. N. J. Persson, *Phys. Rev. B: Condens. Matter Mater. Phys.*, 2004, **70**, 125407.
13 G. Carbone and P. Decuzzi, *J. Appl. Phys.*, 2004, **95**, 4476–4482.
14 B. N. J. Persson, O. Albohr, U. Tartaglino, A. I. Volokitin and E. Tosatti, *J. Phys.: Condens. Matter*, 2005, **17**, R1–R62.
15 M. Scherge and S. Gorb, *Biological Micro- and Nano-Tribology*, Springer, Berlin, 2001.
16 S. Kim and M. Sitti, *Appl. Phys. Lett.*, 2006, **89**, 261911.
17 M. Varenberg, N. M. Pugno and S. Gorb, *Soft Matter*, 2010, **6**, 3269–3272.
18 M. Varenberg and S. Gorb, *J. R. Soc. Interface*, 2008, **5**, 785–789.
19 M. K. Kwak, H.-E. Jeong, W.-G. Bae, H.-S. Jung and K. Y. Suh, *Small*, 2011, **7**, 2296–2300.
20 W. L. Noderer, L. Shen, S. Vajpayee, N. J. Glassmaker, A. Jagota and C.-Y. Hui, *Proc. R. Soc. London, Ser. A*, 2007, **463**, 2631–2654.
21 N. J. Glassmaker, A. Jagota, C.-Y. Hui, W. L. Noderer and M. K. Chaudhury, *Proc. Natl. Acad. Sci. U. S. A.*, 2007, **104**, 10786–10791.
22 M. P. Murphy, S. Kim and M. Sitti, *ACS Appl. Mater. Interfaces*, 2009, **1**(4), 849–855.
23 A. V. Spuskanyuk, R. M. McMeeking, V. S. Deshpande and E. Arzt, *Acta Biomater.*, 2008, **4**, 1669–1676.
24 K. A. Daltorio, S. Gorb, A. Peressadko, A. D. Horchler, R. E. Ritzmann and R. D. Quinn, *Proc.Int. Conf. Climbing and Walking Robots*, 2005, pp. 131–138.
25 S. N. Gorb and M. Varenberg, *J. Adhes. Sci. Technol.*, 2007, **21**, 1175–1183.
26 M. Varenberg and S. Gorb, *J. R. Soc. Interface*, 2007, **4**, 721–725.
27 G. Carbone, E. Pierro and S. Gorb, *Soft Matter*, 2011, **7**, 5545–5552.
28 G. Carbone and E. Pierro, *Small*, 2012, **8**(9), 1449–1454.
29 J. M. Karp and R. Langer, *Nature*, 2011, **477**, 42–43.
30 M. K. Kwak, H.-E. Jeong and K. Y. Suh, *Adv. Mater.*, 2011, **23**(34), 3949–3953.
31 M. Varenberg and S. Gorb, *J. R. Soc. Interface*, 2008, **5**, 383–385.
32 S. Gorb, M. Varenberg, A. Peressadko and J. Tuma, *J. R. Soc. Interface*, 2007, **4**, 271–275.
33 S. Gorb, private communication.
34 L. Heepe, M. Varenberg, Y. Itovich and S. N. Gorb, *J. R. Soc. Interface*, 2011, **8**, 585–589.
35 D. Maugis, *Contact, Adhesion and Rupture of Elastic Solids, Springer Series in Solid State Sciences*, Springer-Verlag, Berlin, Heidlberg, New-York, 1999.
36 G. Carbone and L. Mangialardi, *J. Mech. Phys. Solids*, 2008, **56**(2), 684–706.
37 H. B. Callen, *Thermodynamics and an Introduction to Thermostatistics*, John Wiley & Sons Inc., USA, ISBN Q-471-86256-8, 1985.
38 K. L. Johnson, K. Kendall and A. D. Roberts, *Proc. R. Soc. London, Ser. A*, 1971, **324**, 301–313.

Addition and correction

Note from RSC Publishing

This article was originally published with incorrect page numbers. This is the corrected, final version.

The Royal Society of Chemistry apologises for these errors and any consequent inconvenience to authors and readers.